PASJ: Publ. Astron. Soc. Japan **60**, 935–950, 2008 October 25

Dual-Beam Delay Calibration for VERA

Mareki HONMA,[1,2] Masachika KIJIMA,[1,2] Hiroshi SUDA,[1,3] Noriyuki KAWAGUCHI,[1,2] Hideyuki KOBAYASHI,[1,3,4] Takeshi BUSHIMATA,[1,5] Rie SHIMIZU,[6] Akane YOSHIMURA,[6] Tetsuo SASAO,[7,8] Tomoya HIROTA,[1] Hiroshi IMAI,[6] Kenzaburo IWADATE,[4] Takaaki JIKE,[4] Osamu KAMEYA,[2,4] Ryuichi KAMOHARA,[1] Seisuke KUJI,[4] Tomoharu KURAYAMA,[1] Seiji MANABE,[2,4] Takeshi MIYAJI,[1] Akiharu NAKAGAWA,[6] Toshihiro OMODAKA,[6] Tomoaki OYAMA,[1] Satoshi SAKAI,[4] Katsuhisa SATO,[4] Katsunori M. SHIBATA,[1] and Yoshiaki TAMURA[2,4]

[1]*Mizusawa VERA Observatory, National Astronomical Observatory of Japan, 2-21-1 Osawa, Mitaka, Tokyo 181-8588*

[2]*School of Physical Sciences, Graduate University for Advanced Studies, 2-21-1 Osawa, Mitaka, Tokyo 181-8588*

[3]*Department of Astronomy, The University of Tokyo, 7-3-1 Hongo, Bunkyo-ku, Tokyo 113-0033*

[4]*Mizusawa VERA Observatory, National Astronomical Observatory of Japan, 2-12 Hoshigaoka-cho, Mizusawa-ku, Oshu, Iwate 023-0861*

[5]*Space VLBI Project, National Astronomical Observatory of Japan, 2-21-1 Osawa, Mitaka, Tokyo 181-8588*

[6]*Department fo Physics, Faculty of Science, Kagoshima University, 1-21-35 Korimoto, Kagoshima, Kagoshima 890-0065*

[7]*Ajou University, Suwon 443-749, Republic of Korea*

[8]*Korean VLBI Network, Korean Astronomy and Space Science Institute, Seoul 120-749, Republic of Korea*

mareki.honma@nao.ac.jp

(Received 2008 March 5; accepted 2008 August 19)

Abstract

We present the technique of instrumental delay calibration for the dual-beam system of VLBI Exploration of Radio Astrometry (VERA), namely, the horn-on-dish method, in which artificial noise sources are mounted on the antenna feedome base and a wide-band radio noise is injected into the dual-beam receivers after reflection by a subreflector. We introduce the basic concept of calibration with the horn-on-dish method, and also present results of the experiments to evaluate its calibration accuracy. Detailed comparisons between model path calculations and measured paths from the noise sources show that the horn-on-dish method can calibrate the dual-beam delay difference in the antenna structure and receiver within an $\sim$0.1 mm level. We estimated that the systematic error in the calibration does not exceed 0.127 mm, which was evaluated at an elevation angle of 15°. This error corresponds to an astrometric error of $\sim$11 μas with VERA's maximum baseline. An experimental confirmation of the systematic error in the horn-on-dish method has also been obtained by using a pair of 10 m and VERA's 20 m antennas at the Mizusawa station, demonstrating that the systematic difference between the dual-beam delay difference measured with noise sources and that for celestial objects was 0.118 mm, being consistent with the above estimate.

Key words: astrometry — instrumentation: interferometers — techniques: interferometric

1. Introduction

VERA (VLBI Exploration of Radio Astrometry) is a Japanese VLBI array dedicated to phase-referencing VLBI astrometry to explore the 3D structure of the Milky Way with a target accuracy of 10 μas level (Honma et al. 2000; Kobayashi et al. 2008). The unique feature of VERA is a dual-beam system, in which two independent receivers are located at the focal plane of a Cassegrain antenna. This dual-beam system allows one to observe two adjacent sources (target maser and reference extragalactic sources, within 2.°2 separation) so as to cancel tropospheric fluctuations out. While this system works well for reducing phase fluctuations caused by the troposphere (e.g., Honma et al. 2003), the use of two independent receivers introduces an instrumental delay difference between the dual beams (hereafter dual-beam delay difference), which should be calibrated based on other measurements. In order to calibrate the dual-beam delay difference, in VERA we utilize a horn-on-dish method (Kawaguchi et al. 2000). In this method, four noise sources are mounted on the feedome base of the telescope at each station, and a wide-band noise is emitted toward the subreflector. After reflection by the subreflector, the common wide-band noise is injected into the dual-beam receivers, and by monitoring the correlation between the dual beams, one can monitor a difference in path length between dual-beam receivers and its time variation at the same time as the observations of celestial objects. We note that the basic idea of measuring antenna delay using an artificial radio signal was reported in pioneering work by Otoshi (1981). The main difference between our work and the previous one is that we make use of wide-band continuum noises to attain much higher accuracy, which is $\sim$0.1 mm in path length, being more accurate than the previous one by nearly four orders of magnitude.

The aim of this paper is to present the basic concept of the horn-on-dish method and a detailed evaluation of its validity based on our experiments using the VERA telescopes. The plan of the present paper is as follows. In section 2 we introduce the basic concept of the horn-on-dish method, and in section 3 we present model calculations, which help us to understand the behavior of the dual-beam delay difference. In section 4 we briefly describe the horn-on-dish calibration system installed on the VERA telescope. Next, in section 5,

we report on the experimental results to show that the model and the observed dual-beam delay differences agree with each other, demonstrating that the basic concept of the horn-on-dish method is correct. We also evaluate in section 6 the systematic error in the horn-on-dish method. In section 7 we report on experiments conducted with a pair of antennas at Mizusawa, which provide an independent confirmation of the calibration accuracy of the horn-on-dish method. Finally, in section 8 we discuss the implication of the results presented in this paper for practical radio observations of VERA.

2. Basic Concept

2.1. VLBI Delay Equation

We describe the basic concept of dual-beam delay calibration. For the sake of simplicity, here we consider one-baseline VLBI system, which consists of two dual-beam stations (stations 1 and 2), observing two sources (sources A and B) at the same time. The most important quantity for VLBI astrometry is the geometric delay, which is the difference in the light propagation time from the source to the stations. For instance, the geometric delay for source A can be written as

$$\tau_{\rm g,A} = \frac{\vec{s_{\rm A}} \cdot \vec{B}}{c}, \tag{1}$$

where $\vec{s_{\rm A}}$ is a unit vector toward the source A, $\vec{B}$ the baseline vector (here, for the sake of simplicity we do not consider the effect of a retarded baseline, which causes a higher-order effect), and c the speed of light. The station position is referred to as the AZ–EL crossing point, which is practically the point that has the minimum distance from the azimuth and elevation axes of the telescope.

In practical radio observations, observed delays include some additional delay terms such as instrumental delays and tropospheric ones. The instrumental delay is defined as the difference of the light arrival time at the AZ–EL crossing point and at the actual receiving point, where the voltage of electromagnetic waves is recorded together with the receipt time. Thus, the instrumental delay is caused by electromagnetic wave propagation in the antenna structure, receiver, and transmission cables, as well as by the local oscillator phase and so forth.

Considering the three delay terms described above, namely, geometric, instrumental, and tropospheric delays, we can write the observed delays for sources A and B as

$$\tau_{\rm A} = \tau_{\rm g,A} + (\tau_{\rm atm,A2} - \tau_{\rm atm,A1}) + (\tau_{\rm inst,A2} - \tau_{\rm inst,A1}), \tag{2}$$

$$\tau_{\rm B} = \tau_{\rm g,B} + (\tau_{\rm atm,B2} - \tau_{\rm atm,B1}) + (\tau_{\rm inst,B2} - \tau_{\rm inst,B1}). \tag{3}$$

Here, $\tau_{\rm atm}$ is the tropospheric delay (which includes a rapidly varying term), $\tau_{\rm inst}$ is the instrumental delay term, and subscripts 1 and 2 denote the stations. In a phase-referencing VLBI system like VERA, the two sources are close to each other on the sky plane (i.e., within a few degrees), and hence the tropospheric variations are common to the two sources (i.e., $\tau_{\rm atm,A1} \approx \tau_{\rm atm,B1}$) and are significantly reduced after phase referencing.

Strictly speaking, even after phase referencing, a nearly constant offset still remains in the tropospheric delay term due to the air-mass difference of the two sources, but here we omit this term because its calibration is beyond the scope of this paper (for calibration of the air-mass difference, see, e.g., Honma et al. 2008). Hence, by subtracting the observed delay for source A from that for B, we may obtain

$$\tau_{\rm B} - \tau_{\rm A} = (\tau_{\rm g,B} - \tau_{\rm g,A}) + (\tau_{\rm inst,B2} - \tau_{\rm inst,A2}) - (\tau_{\rm inst,B1} - \tau_{\rm inst,A1}). \tag{4}$$

Here, the instrumental delay terms, such as $(\tau_{\rm inst,B1} - \tau_{\rm inst,A1})$, correspond to the delay difference in the dual beam at each station. Therefore, by measuring the dual-beam delay difference at each station, one can calibrate the instrumental terms in equation (4), and then the geometric delay term, $\tau_{\rm g,B} - \tau_{\rm g,A}$, can be retrieved to obtain the relative positions of the two sources. Thus, the process necessary for dual-beam calibration is to measure the *difference* of the instrumental delay in the dual-beam system, such as $(\tau_{\rm inst,B1} - \tau_{\rm inst,A1})$.

Once the instrumental delays are calibrated and the geometric delay difference between the two sources is obtained, one can obtain the relative source positions of the two sources through the following equation:

$$\tau_{\rm g,B} - \tau_{\rm g,A} = \frac{(\vec{s_{\rm B}} - \vec{s_{\rm A}}) \cdot \vec{B}}{c}. \tag{5}$$

The delay calibration error causes an uncertainty on the left-hand side of equation (5), and is propagated to the error in the relative position vector on the right-hand side as

$$\Delta\tau \approx \frac{|\Delta\vec{s}||\vec{B}|}{c}. \tag{6}$$

Here, $\Delta\tau$ and $\Delta\vec{s}$ are the delay error and the relative position error, respectively. With VERA's maximum baseline length of $|\vec{B}| \approx 2300\,$km and a target accuracy of $|\Delta\vec{s}| \approx 10\,\mu$as, $c\Delta\tau$ should be $\sim 0.1\,$mm, which is the target accuracy of the dual-beam delay calibration in VERA.

2.2. Dual-Beam Delay Difference

Here, we focus on the dual-beam delay difference in each station. First, for the sake of simplicity, we express the dual-beam delay difference as a path length, such as

$$l_{\rm inst,obj} \equiv c(\tau_{\rm inst,B1} - \tau_{\rm inst,A1}). \tag{7}$$

Here, in $l_{\rm inst,obj}$ we omit the subscript for station number because hereafter we only consider the dual-beam delay difference in each station. We also omit the subscript for the beams (A and B) because only the difference (which is always defined as B − A) is considered in the delay calibration (i.e., it is not necessary to know the individual values of $\tau_{\rm inst,A1}$ and $\tau_{\rm inst,B1}$). Note that the subscript "obj" stands for the observed delay difference for a pair of celestial objects, in contrast to the instrumental delay difference measured with noise sources, which will be discussed later, and is denoted by the subscript "NS" throughout this paper.

The term $l_{\rm inst,obj}$ can be further divided into two terms, and we may rewrite it as

$$l_{\rm inst,obj} = l_{\rm ant,obj} + l_{\rm RX}. \tag{8}$$

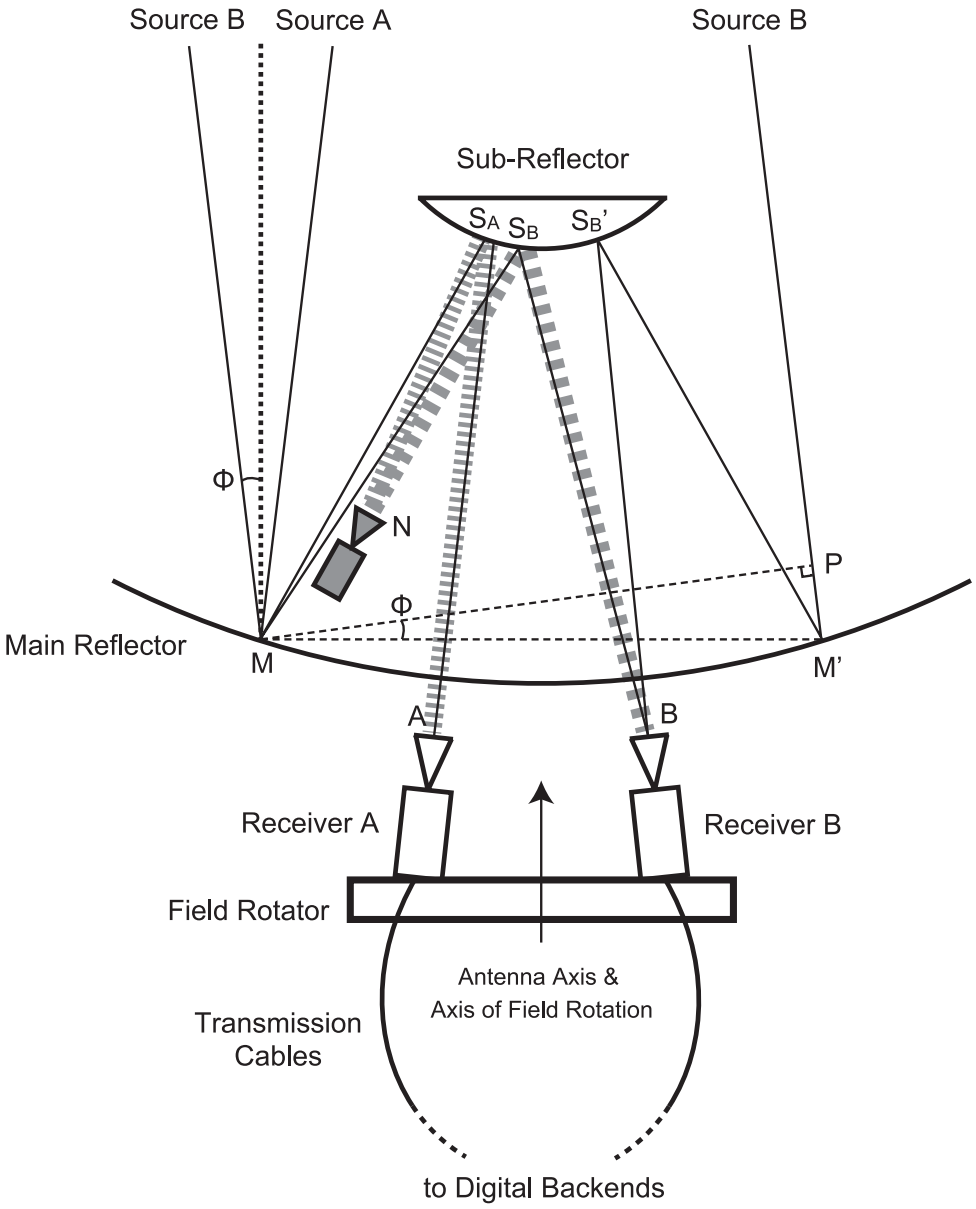

Fig. 1. Schematic view of the radio-wave paths for celestial objects (thin lines) as well as those for a noise source located at point N (thick grey lines) in the dual-beam antenna. For radio waves from celestial objects A and B, representative paths are shown for those reflected at point M on the main reflector. Point M' is symmetric reflection of M with respect to the antenna axis. The dual-beam receivers are mounted on a field rotator, and can be rotated with respect to the antenna axis so that the receivers can follow the apparent source motions caused by Earth rotation. The diameter of the main reflector is 20 m, the diameter of the subreflector 2.6 m, and the distance between the dual-beam receviers for $\phi = 1^\circ$ 1.6 m.

Here, the delay term $l_{\mathrm{ant,obj}}$ corresponds to the path difference caused during electromagnetic wave propagation in the antenna structure (from the main reflector to the receiver feed-horns, i.e., source A–M–S_A–receiver A and source B–M–S_B–receiver B, see figure 1 for schematic view). The term l_{RX} represents the path difference after the receiver feed-horns, including such as difference of the transmission cable lengths from the receivers to the digital backends (where the voltage data are sampled with a time stamp), and also local oscillator phase.

For an ideal dual-beam antenna, which is perfectly symmetric with respect to the antenna axis (including the main- and subreflectors as well as the dual-beam receivers), the term $l_{\mathrm{ant,obj}}$ should be 0, because the paths that occur in the antenna structure (with respect to the AZ–EL crossing point) are the same for the sources A and B, simply because of symmetry. However, in a practical system, $l_{\mathrm{ant,obj}}$ may have a nonzero value due to excess paths caused by a deformation of the main reflector, displacements of the subreflector and the receiver feed-horn, etc. (i.e., deviation from symmetry). For instance, a displacement of the subreflector by 1 mm causes $l_{\mathrm{ant,obj}} = 0.249$ mm, and a displacement of the receiver feed-horn by 1 mm causes $l_{\mathrm{ant,obj}} = 0.141$ mm (see next sections and table 2 for more details), being larger than our target calibration

accuracy of 0.1 mm. Hence, for precise astrometry, $l_{\rm ant,obj}$ should be calibrated based on measurements or predictions.

2.3. Calibration with the Horn-on-Dish Method

The horn-on-dish method (Otoshi 1981; Kawaguchi et al. 2000) is a technique in which artificial noise sources mounted on the antenna are used to monitor the instrumental delay and its variation on real time. In VERA, noise sources are mounted on the antenna feedome base (see figure 2 for the location of noise sources). By monitoring the correlation of the artificial noise received by receivers A and B, one can obtain the dual-beam delay difference and its time variation caused by a displacement of the subreflector and receiver feed-horns as well as any temperature-dependent variations of the transmission cables. What is measured with the noise sources is the dual-beam delay difference in the antenna and the receiver, and by analogy of the dual-beam delay difference for a pair of celestial objects [equation (8)], we can write the dual-beam delay difference for the noise sources, $l_{\rm inst,NS}$, as

$$l_{\rm inst,NS} \equiv l_{\rm ant,NS} + l_{\rm RX}. \tag{9}$$

If the term $l_{\rm inst,NS}$ measured with the noise sources well represents the delay difference for celestial objects, $l_{\rm inst,obj}$, one can calibrate the dual-beam delay difference so as to conduct high-precision astrometry. When equation (8) is compared with (9), the term $l_{\rm RX}$ is common, since the paths for the horn-on-dish noise and radio waves from celestial objects are completely the same through receiver and transmission cables (i.e., path after the receivers A and B in figure 1). In contrast, the difference between paths from a noise source to the receiver feed-horns is not exactly the same as that of radio waves from celestial objects, partly because the horn-on-dish noise does not trace the deformation of the main reflector, itself, and partly because the horn-on-dish noise represents only a part of the subreflector illumination. Thus, the path difference in the antenna measured by the horn-on-dish method ($l_{\rm ant,NS}$) is an approximation of that for celestial objects ($l_{\rm ant,obj}$), and a close approximation is crucial in achieving the target accuracy (this will be tested in later sections).

Another important aspect of the delay difference measured with the horn-on-dish noise is that $l_{\rm inst,NS}$ of equation (9) is not a direct observable quantity of the horn-on-dish method. The observed delay difference includes another bias term, namely,

$$l_{\rm obs,NS} = l_{\rm bias} + l_{\rm ant,NS} + l_{\rm RX}. \tag{10}$$

Here, the term $l_{\rm obs,NS}$ is the difference of paths from the noise source to the digital backends (i.e., difference in length between the following two paths: N–S_A–receiver A–digital backends and N–S_B–receiver B–digital backends, see figure 1). As we discuss in the next subsection, the bias term $l_{\rm bias}$ is purely a geometric effect determined by the relative position of the noise sources with respect to the antenna vertex, and can be precisely predicted once the noise source positions are known.

In summary, when one compares equations (8) and (10) there are two main differences between them: 1) the existence of the bias term $l_{\rm bias}$ for the dual-beam delay difference measured with the noise sources, and 2) the path difference between the radio waves from celestial objects and an artificial noise source (i.e., difference of $l_{\rm ant,obj}$ and $l_{\rm ant,NS}$). Therefore, the key to the measurement of the instrumental delay based on the horn-on-dish method is: 1) to precisely calibrate the bias term, $l_{\rm bias}$, and 2) to reduce the path difference between celestial objects and artificial noise sources (in other words, to better approximate to the object path difference by those of the noise sources).

2.4. Nature of the Bias Term

The bias term $l_{\rm bias}$ in the noise-source path difference is a geometric effect caused by the relative position of the noise source with respect to the antenna vertex. Consider a noise source at point N in figure 1. We note that the noise source position N can be chosen arbitrarily, but, as seen from figure 1, noise sources located closer to the main reflector better represent the radio path for celestial objects. In the VERA system, noise sources are mounted on the feedome base (see figure 2 for a schematic view), being located $\sim$2.2 m away from the antenna axis and $\sim$1.3 m above the main reflector.

In an ideal dual-beam antenna, in which the antenna structure is perfectly symmetric with respect to the antenna axis, the term $l_{\rm ant,NS}$ vanishes, and thus the bias term should be obtained as the path difference from the noise source N to each receiver, namely,

$$l_{\rm bias} \equiv (\overline{\rm NS_B} + \overline{\rm S_B B}) - (\overline{\rm NS_A} + \overline{\rm S_A A}). \tag{11}$$

This equation provides a general definition of the bias term. The most important point is that this is purely geometric effect, and thus $l_{\rm bias}$ can be precisely predicted once the antenna parameters and noise source positions are provided.

In order to provide an order estimate of $l_{\rm bias}$, here we consider a (rather imaginary) noise source located on the main reflector at point M in figure 1. Consider a point M′, which is a symmetric reflection of point M with respect to the antenna axis. Due to the symmetry, it holds that

$$\overline{\rm M'S'_B} + \overline{\rm S'_B B} = \overline{\rm MS_A} + \overline{\rm S_A A}. \tag{12}$$

By combining the above equations, one may obtain

$$l_{\rm bias,0} = (\overline{\rm MS_B} + \overline{\rm S_B B}) - (\overline{\rm M'S'_B} + \overline{\rm S'_B B}), \tag{13}$$

where the subscript "0" denotes that the bias term corresponds to that of a noise source on the main reflector at point M. Since the receiver at point B is on the focal point for source B, the electromagnetic waves from source B reflected at points M and M′ should be in phase at the receiver point B, and thus it requires that

$$\overline{\rm MS_B} + \overline{\rm S_B B} = \overline{\rm PM'} + \overline{\rm M'S'_B} + \overline{\rm S'_B B}. \tag{14}$$

From figure 1, it is clear that $\overline{\rm PM'} = D\sin\phi$, where $D \equiv \overline{\rm MM'}$ and ϕ is the beam offset angle of the source with respect to the antenna axis. Thus, from the above equations one can obtain

$$l_{\rm bias,0} = D\sin\phi. \tag{15}$$

Hence, the bias term can be regarded as a delay gradient at the telescope aperture, defined at points M and M′ on the main reflector. Clearly, $l_{\rm bias,0}$ can be calculated only if the noise source position M is provided. An order estimate of the bias term gives $l_{\rm bias,0} \sim 87$ mm for $D \sim 5$ m and $\phi = 1^\circ$.

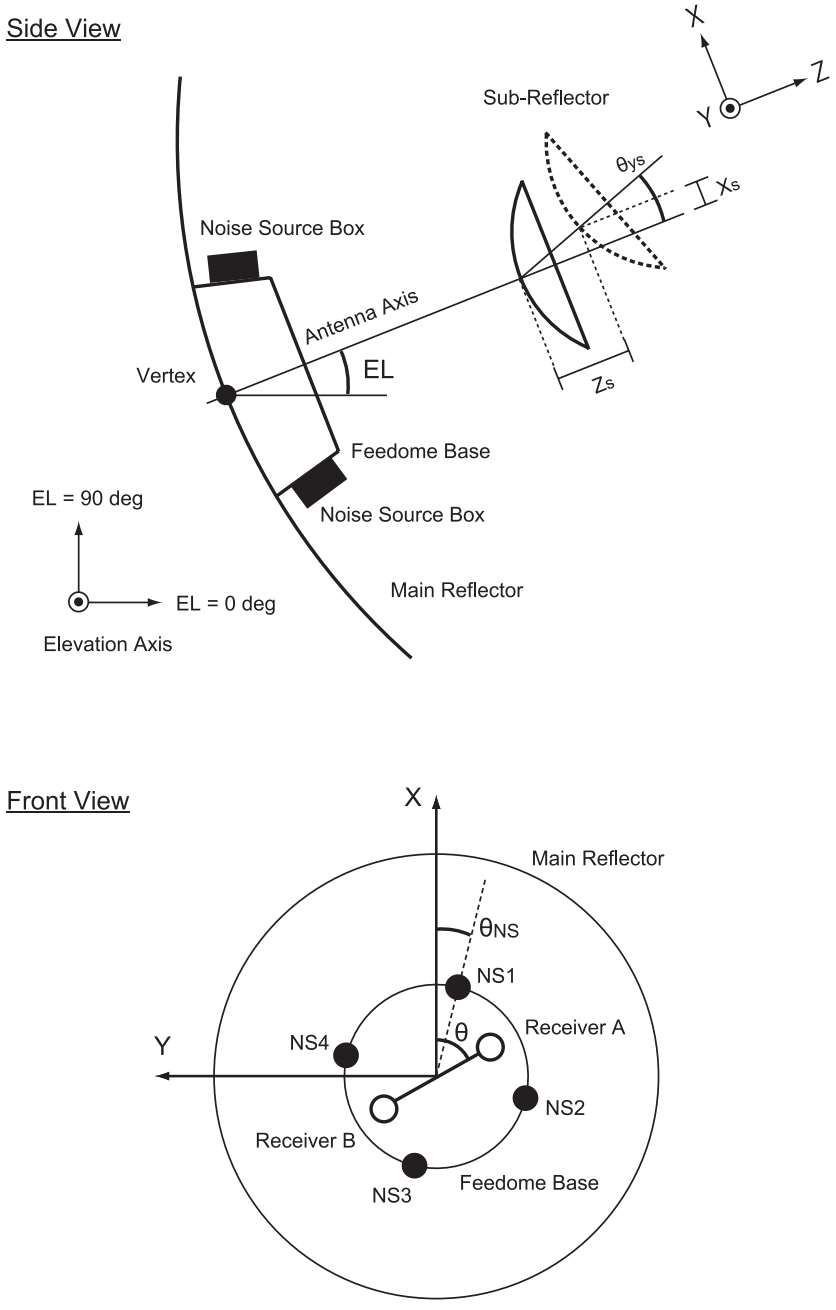

Fig. 2. Schematic view of the antenna, showing the XYZ coordinate system used in this paper. The top panel is a side view of the antenna. The XYZ coordinate system is defined as the right-hand Cartesian coordinate system with the Z axis identical to the antenna axis. Note that the Y axis is identical to the EL axis. An example of subreflector displacement with offsets in $X_{\rm s}$, $Z_{\rm s}$ and $\theta_{\rm Ys}$ is also shown. Bottom panel is the front view of the antenna surface (e.g., seen from the subreflector), showing the field rotation angle θ and the location of noise sources on the feedome base. Distance from the antenna axis to the noise source is 2.2 m, and the noise sources are set on 1.3 m above the main reflector surface.

In practical cases, where the noise sources are located away from the surface of the main reflector (i.e., N in figure 1), the bias term is also determined by the noise source position (i.e., D), and is proportional to $\sin\phi$, similarly in the case of equation (15). Also, during practical radio observations with the dual-beam antenna, the receiver platform rotates so that the receivers can follow diurnal motions. By this rotation, the relative location between receivers A, B, and the noise source changes with time, depending on the field rotation (FR) angle, θ, (see lower part of figure 2 for the definition of the field rotation angle). Thus, in practical cases, the bias term varies as a sinusoidal function of θ, and thus we can write

$$l_{\rm bias} = a \sin\phi \cos(\theta - \theta_{\rm NS}), \tag{16}$$

where a is a function of only the noise source positions and $\theta_{\rm NS}$ is the FR angle offset for noise source position. In later sections, we see that the observed bias terms are indeed described in the form of equation (16).

Table 1. Calculated delay coefficients for noise sources.*

	NS1			NS2			NS3			NS4		
	a (μm)	b (°)	c (μm)	a (μm)	b (°)	c (μm)	a (μm)	b (°)	c (μm)	a (μm)	b (°)	c (μm)
$X_{\rm s}$	262	0.060	0	260	0.045	0	262	−0.269	0	259	0.192	0
$Y_{\rm s}$	260	90.130	0	263	89.745	0	259	90.043	0	262	89.792	0
$Z_{\rm s}$	32	172.758	0	32	82.481	0	32	−7.722	0	33	−96.727	0
$\theta_{\rm Xs}$	66	−89.318	0	71	−90.438	0	65	−89.052	0	70	−89.948	0
$\theta_{\rm Ys}$	70	−0.618	0	65	0.513	0	70	−0.982	0	65	0.555	0
$X_{\rm hA}$	150	179.867	50	151	179.973	−7	150	180.091	−51	151	179.957	6
$Y_{\rm hA}$	150	−90.087	−7	151	−89.840	−51	150	−90.052	6	150	−89.716	50
$Z_{\rm hA}$	6	4.360	999	7	−86.204	999	6	184.317	999	5	93.789	999
$X_{\rm hB}$	150	179.867	−50	151	179.964	7	150	180.091	51	151	179.966	−7
$Y_{\rm hB}$	150	−90.103	7	150	−89.878	51	150	−90.054	−6	151	−89.733	−50
$Z_{\rm hB}$	6	4.356	−999	7	−86.267	−999	6	184.310	−999	5	93.384	−999
Bias	92575	−7.546	0	92582	−97.580	0	92632	172.417	0	92597	82.476	0

* Coefficients a, b, and c for the four noise sources [i.e., equation (19) with j = NS1, NS2, NS3, and NS4]. The listed values correspond to 1 mm displacements in $X_{\rm s}$, $Y_{\rm s}$, ..., or 0.°01 rotations in $\theta_{\rm Xs}$, $\theta_{\rm Ys}$, etc. The coefficients were calculated for the Mizusawa station with $\phi = 1°$ based on the measured noise source positions and the antenna parameters. However, the values listed here are the same as those for other stations because the noise source positions are nearly same among the four stations. Units are μm for a and c, and degree for b.

3. Detailed Modeling of Dual-Beam Delay

In order to understand the behavior of the dual-beam delay difference, here we present model calculations of the path length in the antenna structure. First, as described in section 2, the bias term $l_{\rm bias}$ can be described as a sinusoidal function of the field rotation angle, θ. Thus, we can generally rewrite $l_{\rm bias}$ as

$$l_{{\rm bias},j} = [a_{{\rm bias},j} \cos(\theta - b_{{\rm bias},j})]\phi + c_{{\rm bias},j}. \quad (17)$$

Here, the term $a_{\rm bias}$ is the amplitude of the bias term, and $b_{\rm bias}$ is the phase offset of the field rotation angle, θ. Both $a_{\rm bias}$ and $b_{\rm bias}$ are dependent of j, which is the noise source number (j = NS1, NS2, NS3, and NS4). In contrast to equation (16), the constant offset term, $c_{\rm bias}$, is added to generalize the equation, but basically $c_{\rm bias}$ is 0 for the bias term (the term $c_{\rm bias}$ will be necessary for describing the delay difference caused by antenna deformation, as shown later). We also note that the first term of the right-hand side in equation (17) is proportional to the beam offset angle, ϕ, rather than $\sin\phi$, because we used an approximation of $\phi \approx \sin\phi$. For the maximum separation angle of $\phi = 1.°1$ (or the source pair separation angle of 2.°2), this approximation causes an error of only 6 μm when the maximum amplitude of the bias term ($l_{\rm bias} \sim 90$ mm) is considered. Therefore, the approximation is valid throughout this paper, and the path length difference is proportional to the beam offset angle, ϕ.

In addition to the bias term, the dual-beam delay difference caused in the antenna structure ($l_{\rm ant}$) can also be written as a combination of sinusoidal functions of θ [by analogy with equation (17)], namely,

$$l_{{\rm ant},j} = \sum_i l_{i,j}, \quad (18)$$

$$l_{i,j} = \left\{[a_{i,j} \cos(\theta - b_{i,j})]\phi + c_{i,j}\right\} X_i. \quad (19)$$

Here, the subscript i denotes the components of antenna deformation considered here, and j denotes the celestial object (j = "obj") or the noise source (j = NS1, NS2, NS3, and NS4). For the antenna deformation parameter, X_i, we take into account the following 16 terms: 3 D displacements and rotations of the main-reflector's antenna axis (represented by the best-fit parabola analysis, $X_{\rm m}$, $Y_{\rm m}$, $Z_{\rm m}$, $\theta_{\rm Xm}$, $\theta_{\rm Ym}$), 3 D displacements and rotations of the subreflector ($X_{\rm s}$, $Y_{\rm s}$, $Z_{\rm s}$, $\theta_{\rm Xs}$, $\theta_{\rm Ys}$), and 3 D displacements of the two receiver feed-horns ($X_{\rm hA}$, $Y_{\rm hA}$, $Z_{\rm hA}$, $X_{\rm hB}$, $Y_{\rm hB}$, $Z_{\rm hB}$). The definition of the axis and an example of subreflector displacement are shown in figure 2. Note that the main- and subreflector rotations around the Z axis cause no path-length difference because of axial symmetry of the reflector, and thus it is not necessary to consider $\theta_{\rm Zm}$ or $\theta_{\rm Zs}$. We also note that the effect of the receiver feed-horn rotation is negligible, and thus is not considered here; the beam size of the receiver feed-horn is $\sim 20°$, which is larger than the primary beam of the antenna by two orders of magnitude, and thus the dual-beam delay difference caused by practical feed-horn rotation is negligible (note that the delay difference caused by primary beam rotation is 34 μm for 0.°01 rotation, as listed in table 2).

In order to test how accurately the path difference measured with the horn-on-dish noise sources represents the true path difference for celestial objects, we calculated coefficients a, b, and c in equation (19) based on ray-tracing methods. We used the real parameters of VERA's antenna optics as well as accurately measured positions of noise sources to calculate the path-length difference from the noise sources and the celestial object to the dual-beam receivers. Assuming an offset of 1 mm for displacement and 0.°01 for rotation, the dual-beam delay difference is obtained from the path difference of the rays from the noise source or the celestial object to the dual-beam receivers. The calculations were made with various FR angles with every 30°, and sinusoidal fits were made to obtain the

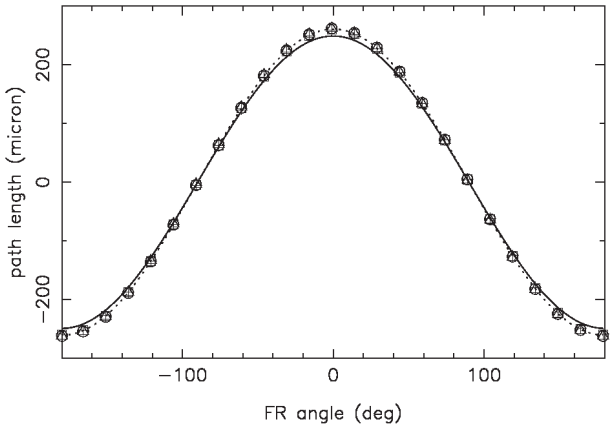

Fig. 3. Calculated dual-beam delay difference caused by a subreflector displacement with $X_{\rm s} = 1\,$mm (for $\phi = 1^\circ$), plotted against the field rotation angle θ. Open circles are for NS1, squares for NS2, triangles for NS3, and crosses for NS4, with every 15° of θ. The dotted curve is the mean of the four noise sources, and the thick curve is the dual-beam delay difference for celestial objects. The delay differences measured with noise sources agree well with that for celestial objects.

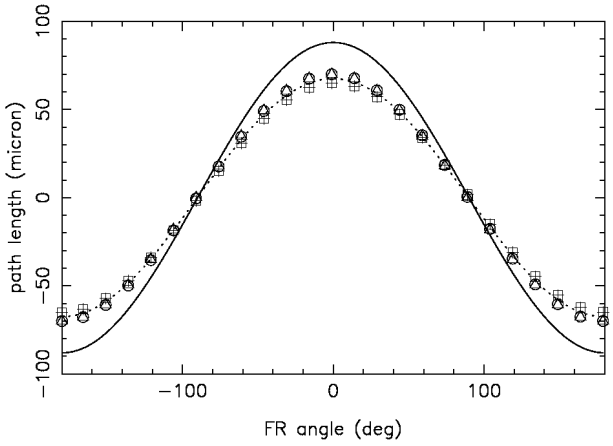

Fig. 4. Same as figure 3, but for a subreflector rotation with $\theta_{\rm Ys} = 0.^\circ01$. The systematic path difference between the noise sources and celestial object (thick curve) is larger than in $X_{\rm s}$ (figure 3), with $\sim 20\,\mu$m at the most.

coefficients a, b, and c in equation (19). To see the dependency on the dual-beam separations, the calculations were made for the beam offset angle of $\phi = 0.^\circ25$, $0.^\circ5$, $0.^\circ75$, and $1.^\circ0$ (corresponding to source separation angle of $0.^\circ5$, $1.^\circ0$, $1.^\circ5$, and $2.^\circ0$). The fitting residuals using equation (19) were at the level of 1–3 μm, and the linearity with respect to ϕ [see equation (19)] was confirmed at the same level.

In table 1 we show the calculated coefficients for the noise source paths, and in table 2 those for celestial objects, both with $\phi = 1.^\circ0$. We note that the results given in tables 1 and 2 were calculated by using the noise source positions at the Mizusawa station. However, except for the bias terms (which slightly vary from station to station, depending on the noise source positions), the values listed in tables 1 and 2 are identical to those for other stations. The listed values correspond to 1 mm displacements in $X_{\rm s}$, $Y_{\rm s}$, ..., or $0.^\circ01$ rotation in $\theta_{\rm Xs}$, $\theta_{\rm Ys}$, ..., etc. Table 1 shows the values for 11 components of the

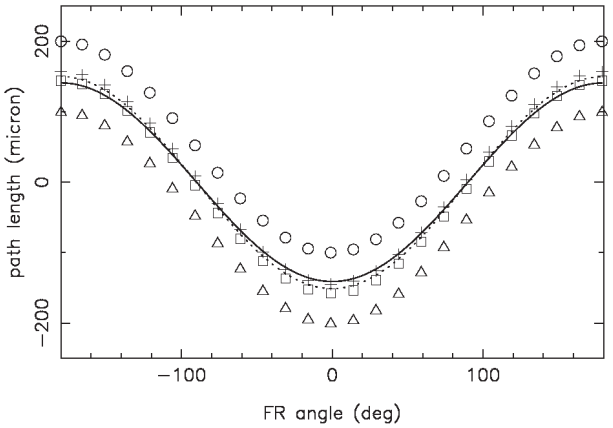

Fig. 5. Same as figure 3, but for a feed-horn displacement with $X_{\rm hA} = 1\,$mm. While systematic offsets among noise sources are remarkable, the mean (dotted curve) is sufficiently close to the dual-beam delay difference for celestial objects (thick curve).

antenna deformation, caused by subreflector and receiver feed-horn displacements. As we have already described, the noise sources cannot trace the dual-beam delay difference caused by the main reflector, and thus there are no coefficients related to the main-reflector deformation in table 1. In contrast, in addition to the 11 components considered in table 1, five more components caused by main-reflector displacements are included in table 2. From tables 1 and 2, one can see the amplitudes of the dual-beam delay differences caused by antenna deformation. For example, in table 2, the amplitude (a) for $X_{\rm s}$ and $Y_{\rm s}$ is 249 μm for a 1 mm displacement for celestial objects, and that for $X_{\rm hA}$ and $Y_{\rm hA}$ is 141 μm for a 1 mm displacement. Thus, a few mm displacement indeed causes an instrumental delay difference larger than the target calibration accuracy of 0.1 mm, and thus such an effect should certainly be calibrated. However, from table 1, one can see that the trend of the dual-beam delay difference for noise sources is similar to that for celestial objects. For instance, for noise sources the amplitudes for $X_{\rm s}$ and $Y_{\rm s}$ are $\sim 260\,\mu$m, and those for $X_{\rm hA}$ and $Y_{\rm hA}$ are 150 μm, being close to those for celestial objects. Note that in tables 1 and 2, the dual-beam delay difference caused by the feed-horn displacement in the Z direction ($Z_{\rm hA}$, $Z_{\rm hB}$) shows an exceptional behavior, in which the term c is dominating, and thus is nearly constant against the field rotation angle, θ. This can be easily understood because the direction of wave propagation from the subreflector to the receiver horn is nearly parallel to the Z axis (see figure 1), and thus the horn displacement along the Z axis causes a constant offset in the path difference.

To illustrate some representative cases of the dependence of delay differences on θ, we show the variation of $l_{i,j}$ for $X_{\rm s}$, $\theta_{\rm Ys}$, and $X_{\rm hA}$ in figures 3–5. We note that the plots for $Y_{\rm s}$, $\theta_{\rm Xs}$, and $Y_{\rm hA}$ should be the same as those for $X_{\rm s}$, $\theta_{\rm Ys}$, and $X_{\rm hA}$ in figures 3–5 except for a phase (b term) difference of 90°; also note that $X_{\rm hB}$ and $Y_{\rm hB}$ are the same as those for $X_{\rm hA}$ and $Y_{\rm hA}$. In figures 3–5, $l_{i,j}$ for four noise sources are plotted with symbols (open circle, square, triangle, and cross from NS1 to NS4). Also shown in figures 3–5 are the mean of the delay difference obtained by four noise sources

Table 2. Calculated delay coefficients for celestial objects.*

	a (μm)	b (°)	c (μm)	$a_{\rm NS1-4}$ (μm)	$b_{\rm NS1-4}$ (°)	$c_{\rm NS1-4}$ (μm)	Δa (μm)	Δc (μm)
$X_{\rm s}$	249	0.000	0	261	0.006	0	−12	0
$Y_{\rm s}$	249	90.000	0	261	89.927	0	−12	0
$Z_{\rm s}$	0	0.000	0	0	0.000	0	0	0
$\theta_{\rm Xs}$	88	−90.000	0	68	−89.709	0	20	0
$\theta_{\rm Ys}$	88	0.000	0	67	−0.159	0	21	0
$X_{\rm hA}$	141	180.000	0	150	179.972	0	−9	0
$Y_{\rm hA}$	141	−90.000	0	150	−89.924	0	−9	0
$Z_{\rm hA}$	−2	180.000	993	0	0.000	999	−2	−6
$X_{\rm hB}$	141	180.000	0	150	179.972	0	−9	0
$Y_{\rm hB}$	141	−90.000	0	150	−89.942	0	−9	0
$Z_{\rm hB}$	−2	180.000	−993	0	0.000	−999	−2	6
Bias	0	0.000	0	—	—	—	—	—
$X_{\rm m}$	17	0.000	0	—	—	—	—	—
$Y_{\rm m}$	17	90.000	0	—	—	—	—	—
$Z_{\rm m}$	0	0.000	0	—	—	—	—	—
$\theta_{\rm Xm}$	34	−90.000	0	—	—	—	—	—
$\theta_{\rm Ym}$	34	0.000	0	—	—	—	—	—

* Coefficients a, b, and c for celestial objects [i.e., equation (19) with $j =$ "obj"]. Same as in table 1, the listed values correspond to 1 mm displacements in $X_{\rm s}$, $Y_{\rm s}$, ..., or 0.°01 rotations in $\theta_{\rm Xs}$, $\theta_{\rm Ys}$, etc. The coefficients were calculated for the Mizusawa station with $\phi = 1°$ based on the measured noise source positions. Units are μm for a and c, and degree for b. Also listed are the coefficients for the mean of the four noise sources ($a_{\rm NS1-4}$, $b_{\rm NS1-4}$, and $c_{\rm NS1-4}$) and the difference of the a and c terms between celestial objects and the noise source mean (Δa and Δc).

(dotted curve) and the dual-beam delay difference for celestial objects (thick curve). For $X_{\rm s} = 1$ mm in figure 3, the delay differences for noise sources are in agreement with that for celestial objects, with the maximum difference of 12 μm, which is 5% of the amplitude ($a \approx 260\,\mu$m). For $\theta_{\rm Ys} = 0.°01$ (figure 4), the trend is similar to that for $X_{\rm s} = 1$ mm, but the maximum difference is somewhat larger, being $\sim$21 μm, corresponding to $\sim$25% of the amplitude, a. This is clearly seen in figure 4 as a difference in amplitude between the thick curve (celestial object) and the dotted curve (mean of the noise sources). The most notable differences are seen in the plot for $X_{\rm hA} = 1$ mm (figure 5), where the path difference traced with each noise source has a constant offset, differing by $\sim \pm 50\,\mu$m at the most. Hence, at least the path difference caused by $X_{\rm hA}$ (or similarly by $Y_{\rm hA}$, $X_{\rm hB}$, and $Y_{\rm hB}$), which is calibrated with only one noise source, could cause a systematic offset of $\sim 50\,\mu$m for a 1 mm displacement. However, if we use multiple noise sources which are located axisymmetrically around the antenna axis, the averaged path difference is fairly close to that for the celestial objects (dotted line in figure 5). This is the main reason why we used four noise sources instead of one (in other words, to make $l_{\rm inst,NS}$ closer to $l_{\rm inst,obj}$).

In table 2 we also show a comparison of dual-beam delay differences for celestial objects and the mean of the four noise sources. As shown in table 2, the maximum deviations are 12 μm for $X_{\rm s}$ and $Y_{\rm s} = 1$ mm, $\sim$20 μm for $\theta_{\rm Xs}$ and $\theta_{\rm Ys} = 0.°01$, 9 μm for $X_{\rm hA}$, $Y_{\rm hA}$, $X_{\rm hB}$, and $Y_{\rm hB} = 1$ mm, and 8 μm for $Z_{\rm hA}$ and $Z_{\rm hB} = 1$ mm. Thus, from the above calculations, one can expect that dual-beam delay differences measured with noise sources indeed trace those for celestial objects, as long as the displacements of the subreflector and the feed-horns are on a few mm scale (or a few times 0.°01 as a rotation), which are typical values of antenna deformations.

As already mentioned above, the noise sources cannot trace the dual-beam delay difference caused by the deformation of the main reflector, and thus this term can cause a systematic error in our calibration system using the horn-on-dish method. In table 2, one can see amplitudes of the systematic error, being $\sim$20–30 μm for 1 mm or 0.°01 displacements of the antenna focus. These values are smaller than those caused by subreflector displacements by nearly an order of magnitude, and the dual-beam delay difference caused by main-reflector deformation is within an acceptable range when compared to the target calibration accuracy of 0.1 mm. Details of these systematic effects are further discussed in section 6.

4. Dual-Beam Delay Calibration System

In this section, we briefly summarize the horn-on-dish calibration system installed onto the VERA antenna. At each station, four artificial noise sources are located on the feedome base, which has a diameter of $\sim$4.4 m and is located on the main reflector (see figure 2 for a schematic view). The locations of four noise source boxes are axisymmetric with respect to the antenna axis (i.e., 90° separation of the field rotation angle θ), and each box contains two noise-emitting systems, those for the K and Q bands, respectively. The noise-emitting system consists of a conical horn, a noise generator [calibrated noise diode with a known excess noise ratio (ENR), which is typically 20–25 dB], an amplifier, and a manually adjustable attenuator, so that the noise injection level can be

optimized. In order to calibrate the bias term ($l_{\rm bias}$), the positions of the noise source boxes were accurately (higher than $\sim$1 mm) measured with respect to the antenna vertex based on an electronic distance meter as well as a photogrammetry technique. Also, the positions of the noise-emitting horns were measured with respect to the noise source boxes based on 3 D CMM (Coordinate Measuring Machine), so that the horn position with respect to the antenna vertex can be known.

The artificial wide-band noise, emitted from the noise source box, is reflected by the subreflector and injected into the two receivers located on the dual-beam platform. The typical injection level (in terms of the system noise temperature) is 5–7 K for the K band and 10–15 K for the Q band. Since the typical system noise temperature is 150 K for the K band and 350 K for the Q band, the system temperature increase by the calibration noise is not significant, being a few percent. The injected noise is amplified in the dual-beam receivers, and then down-converted to the baseband, ranging over 0–512 MHz. Note that these frequency conversion processes are common to those for signals from celestial objects, and thus the noise path is completely the same as those for celestial objects after the receiver to the digital backends [corresponding to the $l_{\rm RX}$ term in equations (8) and (9)]. The baseband output of each receiver is digitized at a bit rate of 2048 Mbps (megabit per second) with two-bit quantization, and is sent from the receiver cabin to the antenna control building, where the real-time correlator is located. The correlator is an XF-type lag-correlator designed by Elecs Industry Co., with a capability for a real-time correlation between the two beams to provide correlated data of 1024 spectral channels per bandwidth (512 MHz) at an accumulation period of 1 s. For an injected noise of 5 K, a system noise temperature of 150 K (for the K band), and a bandwidth of 512 MHz, an integration for 1 s provides an S/N ratio of 700 or higher for the calibration noise, which is high enough for path-length measurements with an accuracy of $\sim$20 μm. This S/N ratio is also high enough to solve the $2\pi N$ ambiguity in the phase delay; the required S/N is roughly estimated as the ratio of the radio frequency to the bandwidth, i.e., 22 GHz/512 MHz $\approx$43 for the K band and 43 GHz/512 MHz $\approx$84 for the Q band.

5. Comparison between the Model and Observations

In order to evaluate the validity of the calibration with the horn-on-dish method, we compare the dual-beam delay differences measured with the horn-on-dish method to those predicted from model calculations. Here, we present two examples of a validity check: 1) measurements of the delay difference caused by a receiver feed-horn displacement, and 2) comparisons of the predicted and measured values of the total path differences in the antenna structure.

5.1. Feed-Horn Displacements

In VERA's dual-beam system, the receivers are mounted on a Stewart-mount platform, which is steerable to locate the feed-horn at its correct position (i.e., along the focal plane for a pair separation angle ranging from 0.°3 to 2.°2). Therefore, by actively changing the feed-horn position one can trace how the dual-beam delay difference varies, and by comparing the measured delay difference with the model calculations, one can test the validity of the model. Figure 6 shows an example of such measurements made at the Mizusawa station. The data were taken on 2002 November 15 with the following observing parameters: K-band (at the radio frequency of 21.8 GHz), NS4, $\phi = 1^\circ$, $\theta = 0^\circ$, and EL $= 90^\circ$ (pointing toward the direction to the zenith).

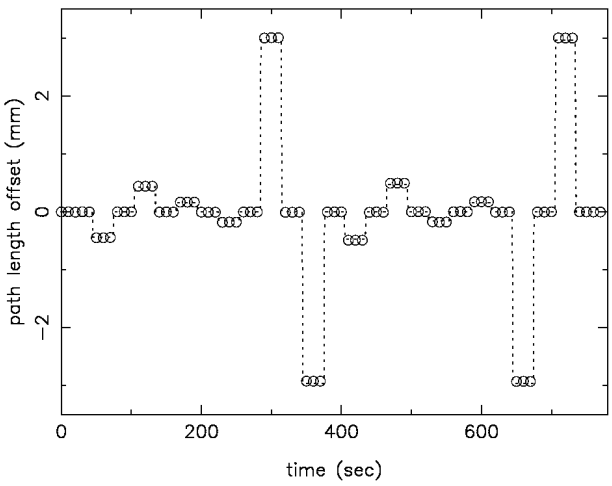

Fig. 6. Examples of a path length variation caused by receiver feed-horn displacements (K-band, NS4, $\phi = 1^\circ$, $\theta = 0^\circ$, Mizusawa station). Open circles show the measurements (every 10 s), and the dotted line shows model predictions. The feed-horn displacement sequence is as follows: 0, $X_{\rm hA} = +3$, 0, -3, 0, $Y_{\rm hA} = +3$, 0, -3, 0, $Z_{\rm hA} = +3$, 0, -3, 0, in mm, and the same for beam B after beam A. The maximum offsets correspond to $Z_{\rm hA}$ and $Z_{\rm hB} = \pm 3$ mm.

The delay-difference variation was monitored while changing the feed-horn positions by adding an offset of $\pm$3 mm to the 6 axes, namely, $X_{\rm hA}$, $Y_{\rm hA}$, $Z_{\rm hA}$, $X_{\rm hB}$, $Y_{\rm hB}$, and $Z_{\rm hB}$, respectively. Note that for each axis measurement, an offset was added to only the axis concerned and no offsets were given to the remaining axes. For each displacement, the delay difference was measured for 30 s, with data points of every 1 s, which is the default integration time of the correlator of the dual-beam calibration system. In figure 6, measurements are plotted every 10 s (by picking up one data point every 10 s just for clarity), and the delay difference variation expected from the model calculations are also plotted (dotted line). Here, the initial delay difference is set to be 0, since we are not interested in the delay difference, itself, but in its variation. In figure 6, the measurements are in complete agreement with the model. The maximum deviation of the measured delay from the model expectations (i.e., using coefficients in table 1) is 35–40 μm for $Z_{\rm hA}$ and $Z_{\rm hB} = \pm 3$ mm, which is $\sim$1% of the path-length change. The rms (root mean square) of the differences between the model predictions and the measurements is 25 μm, which is likely to be dominated by the S/N limit of the noise source system. We note that the measurements presented above were obtained for $\pm$3 mm offsets. For 1 mm displacements (which are summarized in table 1), the rms of the model–measurement difference is $\sim$8 μm, and hence we can conclude that the accuracy of the model calculations given in table 1 is higher than 10 μm. We made such measurements for all four noise sources at the

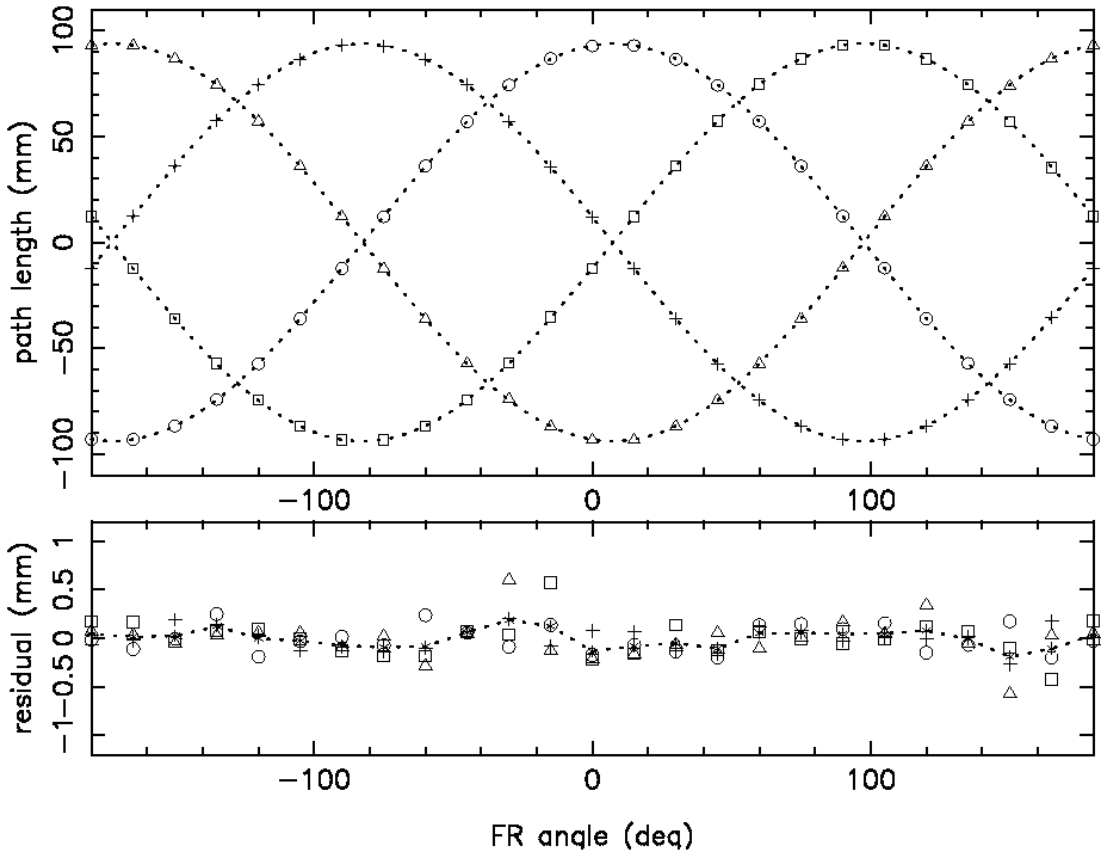

Fig. 7. Examples of the dual-beam delay difference measured with the noise sources, with respect to the field rotation angle, θ. Open circles are for NS1, squares for NS2, triangles for NS3, and crosses for NS4. The top panel shows the measured values with sinusoidal fits to each noise source (dotted curve). Note that constant offsets, $c_{\rm obs}$, which represent the contribution of $l_{\rm RX}$, are eliminated here for clarity. The bottom panel shows the residuals of the fit, with the mean of the four noise sources (dotted curve).

Mizusawa and other stations at both the K and Q bands, and confirmed that the measurements and the model predictions agree well with each other, regardless of the stations, the noise-source positions, or the observing frequencies.

5.2. Total Path Difference in the Antenna Structure

We also compare the delay differences in the antenna structure measured with noise sources to those expected from the model presented in the previous section. As we have already seen in the previous section (e.g., table 1), basically the delay difference for noise sources is dominated by the bias term (an amplitude of 92 mm for $\phi = 1^\circ$). However, there are additional delay terms due to displacements of the subreflector and the receiver feed-horns, which can be described by a sum of the sinusoidal functions [equations (18) and (19)]. Since a sum of sinusoidal functions also becomes sinusoidal, we can fit the total delay difference with a sinusoidal function of θ, namely,

$$l_{{\rm obs},j} = a_{{\rm obs},j} \cos(\theta - b_{{\rm obs},j}) + c_{{\rm obs},j}\,. \tag{20}$$

Figure 7 shows an example of such measurements carried out at the Mizusawa station with $\phi = 1^\circ$ at the K band, taken on 2002 November 15. The measurements were made with a FR angle step of 15° from $\theta = 180^\circ$ to -180°, and at each FR angle the data were integrated for 20 s . During the measurements, the telescope was set to be in the rest position toward the direction to the zenith (EL $= 90^\circ$).

The offset term, $c_{\rm obs}$, which basically corresponds to the path difference between the feed-horns and the digital backends (i.e., $l_{\rm RX}$), is fairly stable during our measurements for a cycle of θ. Hence, in figure 7 the constant offset term, $c_{\rm obs}$, is eliminated so as to extract the dual-beam delay difference in the antenna structure, which corresponds to $l_{\rm bias} + l_{\rm ant,NS}$ in equation (10). In figure 7, the basic trend of the measured path difference is well fitted by equation (20), with amplitudes of $\sim$94 mm (dotted curves). The fitting residuals are also shown in the bottom panel of figure 7. While some measurement points show a deviation of 0.3–0.5 mm, most of the points are within 0.1–0.2 mm of the best-fit sinusoidal curve. The rms of the fitting residual is 165 μm. This residual is larger than that from the S/N ratio of the noise, which is typically 20 μm. We note that there are mainly two reasons for the deviations from ideal sinusoidal curves: 1) a real fluctuation of the delay difference caused by, for instance, small mechanical fluctuations of the dual-beam platform, which varies with θ, and 2) an apparent variation of the delay difference such as those caused by multipath effects of the noise source signal (e.g., interference of NS signal reflected by subreflector stays or somewhere else than the subreflector, itself). We note that the dual-beam delay difference caused by the feed-horn displacements (which originate from mechanical fluctuations) is basically common

Table 3. Comparisons of measured and modeled path differences at the Mizusawa station.*

	$a_{\rm obs}$ (mm)	$a_{\rm mod}$ (mm)	Δa (mm)	$b_{\rm obs}$ (°)	$b_{\rm mod}$ (°)	Δb (°)	Δl (mm)
K band							
NS1	93.797	93.716	0.081	7.512	7.480	0.032	0.052
NS2	93.905	93.925	−0.019	97.404	97.537	−0.134	−0.220
NS3	93.893	94.016	−0.123	187.500	187.417	0.083	0.136
NS4	93.839	93.777	0.062	−82.646	−82.664	0.019	0.031
Q band							
NS1	93.615	93.648	−0.033	10.383	10.387	−0.003	−0.005
NS2	93.734	93.665	0.069	100.510	100.514	−0.004	−0.007
NS3	93.843	93.847	−0.004	190.481	190.511	−0.029	−0.048
NS4	93.774	93.807	−0.033	−79.610	−79.647	0.037	0.061
rms			0.064			0.060	0.098

* Measured and modeled coefficients a and b of the path difference in the antenna structure at the Mizusawa stations, with $\phi = 1°$ and for both the K and Q bands [i.e., equations (20) and (24)]. Note that the difference of the two coefficients is defined as $\Delta a \equiv a_{\rm obs} - a_{\rm mod}$, and the same for Δb. Also note that Δl is the path difference caused by Δb, which is given by $\Delta l = a \sin(\Delta b)$. Units are mm for a and Δl, and degree for b.

to the four noise sources, and thus can be traced by taking the mean of the dual-beam delay differences for the four noise sources. On the other hand, if the apparent variation of the delay difference is caused by the multipath effect, it should vary according to the noise source position as well as the field rotation angle, θ, and hence their distributions are likely to be random. To see the effects of the mechanical fluctuations in the bottom panel of figure 7, we also plotted the mean of the fitting residuals for the four noise sources (dotted line). The rms of the residual mean (with respect to variation of θ) is found to be 90 μm. Hence, the fitting residual rms of 165 μm (for each noise sources) is likely to be a combination of the real mechanical fluctuation of 90 μm and the apparent delay variation (such as those caused by multipath interference), whose contribution is expected to be 138 μm [$\approx \sqrt{(165^2 - 90^2)}$]. The effect of the systematic errors on the total calibration accuracy is discussed in the next section.

To compare the above measurements with the models given in section 3, we modeled the dual-beam delay difference in the antenna structure on a combination of antenna displacement components and the bias term, as follows:

$$l_{{\rm mod},j} = l_{{\rm bias},j} + l_{{\rm ant},j} = l_{{\rm bias},j} + \sum_i l_{i,j}. \tag{21}$$

The displacements of the subreflector and the receiver feedhorn (i.e., values of $X_{\rm s}$, $Y_{\rm s}$, ...) were measured at the antenna site, based on an electronic distance meter as well as photogrammetry with an accuracy of $\sim$1 mm or higher. With the measured values of $X_{\rm s}$, $Y_{\rm s}$, ... as well as the noise source positions, the model path difference can be calculated by using the coefficients a, b, and c, listed in table 1.

By considering all of the necessary terms given in table 1, we can explicitly rewrite equation (21) as

$$\begin{aligned} l_{\rm mod} = \phi \times \big[& (a_{\rm bias} - a_{\rm Zs} Z_{\rm s}) \cos(\theta - \theta_{\rm NS}) \\ & + (a_{\rm Xs} X_{\rm s} + a_{\theta_{\rm Ys}} \theta_{\rm Ys} - a_{\rm X_{hA}} X_{\rm hA} - a_{\rm X_{hB}} X_{\rm hB}) \cos\theta \\ & + (a_{\rm Ys} Y_{\rm s} - a_{\theta_{\rm Xs}} \theta_{\rm Xs} - a_{\rm Y_{hA}} Y_{\rm hA} - a_{\rm Y_{hB}} Y_{\rm hB}) \sin\theta \big] \\ & + c_{\rm X_{hA}} X_{\rm hA} + c_{\rm X_{hB}} X_{\rm hB} \\ & + c_{\rm Y_{hA}} Y_{\rm hA} + c_{\rm Y_{hB}} Y_{\rm hB} \\ & + c_{\rm Z_{hA}} Z_{\rm hA} + c_{\rm Z_{hB}} Z_{\rm hB}, \end{aligned} \tag{22}$$

where the subscript j (which describes the noise source number) is omitted. Here, we also omitted a terms for $Z_{\rm hA}$ and $Z_{\rm hB}$, which are $\sim$6 μm, and c terms for $X_{\rm s}$, $Y_{\rm s}$, $Z_{\rm s}$, $\theta_{\rm Xs}$, and $\theta_{\rm Ys}$, which are essentially 0 (see table 1). As we already described, coefficients a, b, and c are given in the previous section, and the displacements ($X_{\rm s}$, $Y_{\rm s}$, ...) are measured, and thus are already known. However, there are two parameters that should be taken as "unknown" and thus to be solved here, which are the beam-offset angle, ϕ, and the field rotation angle, θ. Basically their values should be known *a priori*, so that we can send a command to the telescope to set the dual-beam receivers at their correct positions. However, in practice, it is possible that the "command value" and the "real value" can be slightly different, for instance, due to an angular offset in the encoder. To eliminate such an error from this, it is better to solve ϕ and θ from our measurements, rather than simply using the "command value".

The real values of the beam-offset angle and the field rotation angle, which we denote as ϕ' and θ', can be obtained based on the axisymmetric location of the noise sources (e.g., $\theta_{\rm NS1} \approx \theta_{\rm NS3} - 180°$ and $\theta_{\rm NS2} \approx \theta_{\rm NS4} - 180°$, with an approximation accuracy of higher than 0.°05). If we subtract $l_{\rm mod}$ for the noise source 3 from $l_{\rm mod}$ for 1, we can then obtain

$$\begin{aligned} & l_{\rm mod,NS1} - l_{\rm mod,NS3} \\ & = \phi' \times \big[(a_{\rm bias,NS1} - a_{\rm Zs} Z_{\rm s}) \cos(\theta' - \theta_{\rm NS1}) \\ & \qquad - (a_{\rm bias,NS3} - a_{\rm Zs} Z_{\rm s}) \cos(\theta' - \theta_{\rm NS3}) \big] \\ & \approx \big[(a_{\rm bias,NS1} + a_{\rm bias,NS3} - 2 a_{\rm Zs} Z_{\rm s}) \cos(\theta' - \theta_{\rm NS1}) \big] \phi'. \end{aligned} \tag{23}$$

The important point here is that, as can be seen in table 1, the dual-beam delay differences caused by antenna deformations [those in equation (22)] are common to NS1 and NS3

(and the same applies to another pair of noise sources) due to symmetry, and thus vanish in equation (23). Then, one can directly compare equation (23) with the observations (i.e., $l_{\rm obs,NS1} - l_{\rm obs,NS3}$) to obtain the real values of the beam offset angle, ϕ, and the field rotation angle, θ. This method was applied to the data for all four stations, and angular offsets in each axis (i.e., $\Delta\theta \equiv \theta' - \theta$ and $\Delta\phi \equiv \phi' - \phi$) were determined. Typical values are $\Delta\theta \sim 0.^\circ1$ and $\Delta\phi$ of $0.^\circ004$ to $0.^\circ008$ for $\phi = 1^\circ$. These terms should cause pointing errors of $6''$–$15''$ at each beam when celestial objects are observed with this offset angle. This is consistent with our pointing measurements, which certainly show this kind of pointing offset.[1]

Using the measured displacements (i.e., $X_{\rm s}$, $Y_{\rm s}$, ...), the coefficients a, b, and c given in table 1, and the angular offsets in ϕ and θ obtained above, we finally obtained the model delay difference for each noise source. Similarly in the case of equation (20), the model delay difference was also fitted with a sinusoidal function of the field rotation angle, θ, as

$$l_{{\rm mod},j} = a_{{\rm mod},j} \cos(\theta - b_{{\rm mod},j}) + c_{{\rm mod},j}, \quad (24)$$

to obtain the coefficients $a_{\rm mod}$ and $b_{\rm mod}$. Here, the term $c_{\rm mod}$ was not compared with the measurements ($c_{\rm obs}$), because the term $c_{\rm obs}$ contains unpredictable components, such as the transmission cable length and the local oscillator phase, which are not related to the path difference in the antenna structure. Table 3 summarizes comparisons of the measured and modeled coefficients, a and b, for the Mizusawa station with a beam offset angle of $\phi = 1^\circ$, for both the K and Q bands. From table 3, one can see that the measured path differences are in agreement with the models. For instance, the differences in amplitude (i.e., $\Delta a \equiv a_{\rm obs} - a_{\rm mod}$) are mostly less than 0.1 mm. In fact, in table 3, the rms value of Δa for the eight cases (4 noise sources times 2 bands) is 64 μm. Also, the rms value of Δb for the eight cases is $0.^\circ060$. When one considers an amplitude a of $\sim$94 mm for the $\phi = 1^\circ$ case, the error in b causes a path-difference error of $\sim 98\,\mu$m ($\approx a$ sin Δb). We also made the same comparisons for different beam offset angles of $0.^\circ25$, $0.^\circ5$, $0.^\circ75$, and $1.^\circ0$ for all of the four stations of VERA, both in the K and Q bands. The rms value of Δa for all data (128 samples: 4 stations, 4 noise sources, 4 separation angles, and 2 bands) is 56 μm, which is similar to that of the Mizusawa station (in table 3). Also, for all data of 128 samples, we obtained the rms of the path length differences caused by Δb to be 85 μm, which is also close to the value for the Mizusawa station. Therefore, the measurements agree with the model within $\sim$0.1 mm of the path length difference, regardless of the stations, observing frequencies, or beam-offset angles, indicating that our understanding of the behavior of the dual-beam delay difference in the antenna structure is correct at the level of $\sim$0.1 mm.

6. Total Calibration Error

Here, we estimate the total calibration error of the horn-on-dish methods when the dual-beam delay difference was calibrated by using the four noise sources. First, we consider the measurement errors of the dual-beam delay difference. As summarized in section 4, the S/N ratio of the noise sources is $\sim$700 or higher for typical observing conditions, and the expected thermal error is $\sim 20\,\mu$m for 1 s integration. This is much smaller than the errors discussed in the previous sections, which was estimated by the fitting residuals of the path length with a sinusoidal curve (e.g., figure 7). The rms of the fitting residuals in figure 7 was 165 μm and, as we have described, these errors are likely to be a combination of 1) the real delay variation caused by mechanical fluctuations of the dual-beam platform and 2) the apparent delay variation caused by such as multipath effects of the noise source signal. The contributions of these variations were estimated to be 90 and 138 μm, respectively. The former is a real variation of the delay difference traced with the noise sources (which is basically common to celestial objects), and thus is not a source of errors in calibration. On the other hand, the latter term (apparent delay variation) causes an error in the delay calibrations for VERA. As we have described in section 5, the apparent delay variation caused by such a multipath effect could vary with the noise source position and the field rotation angle, θ, and thus can be treated as a random noise, which causes statistical errors. Thus, under the existence of a 138 μm error in the path-difference measurement with each noise source, the error in the path-difference measurements with the four noise sources is expected to be 69 μm ($\approx 138/\sqrt{N_{\rm NS}}$, $N_{\rm NS} = 4$ is the number of noise sources). Thus, we take the statistical error in the path-difference measurement to be $\sigma_{\rm stat} = 69\,\mu$m after taking an average of the four noise sources.

Next we consider the systematic error in our method. As already described, the systematic error in the antenna structure consists of the following two parts: 1) the path difference between the two radio waves from the noise sources and celestial objects (i.e., the difference between $l_{\rm ant,obj}$ and $l_{\rm ant,NS}$), and 2) the delay difference caused by the main-reflector deformation (which cannot be traced by the noise sources). Both effects are the largest at a low elevation angle (EL), where the gravitational deformation reaches a maximum. Here, we estimate the systematic error toward a low-elevation source by using the antenna deformation parameters at an EL of 15°, which is the lowest elevation angle in practical radio observations. We also assume a field rotation angle of $\theta = 0^\circ$, which provides the largest path difference due to gravitational deformation, because in such a configuration the location of the dual-beam receivers is nearly parallel to the vertical line. According to the antenna measurements at the VERA stations, the subreflector and receiver feed-horn displacements are $X_{\rm s} \approx -3$ mm, $\theta_{\rm Ys} \approx 0.^\circ01$, $X_{\rm hA} \approx -1$ mm, and $X_{\rm hB} \approx -4$ mm at EL = 15°, with a typical measurement error of $\sim$1 mm or $\sim 0.^\circ01$. Note that displacements in Y are fairly small, because the Y axis is perpendicular to the vertical line. We also note that the subreflector displacement in the Z direction ($Z_{\rm s}$) is $\sim$2 mm, but as can be seen from table 2 this displacement causes no systematic error. When we combine the subreflector and feed-horn displacement parameters with the coefficients given in tables 1 and 2, the sum of the terms described above ($X_{\rm s}$, $\theta_{\rm Ys}$, $X_{\rm hA}$, and $X_{\rm hB}$) corresponds to a systematic error in the path-difference calibration of $\sigma_{\rm sys,sub} = 12\,\mu$m. As for the main reflector, according to the best-fit parabola analysis at

[1] For pointing measurements, readers can refer to the VERA status report, which can be found at ⟨http://veraserver.mtk.nao.ac.jp/restricted/index-e.html⟩.

EL = 15°, the displacement and rotation of the antenna axis are calculated as $X_{\rm m} \approx -3$ mm and $\theta_{\rm Ym} \approx -0.^{\circ}025$. When these terms are summed up with the coefficients given in table 2, the deformation of the main reflector causes a systematic error of $\sigma_{\rm sys,main} = -136\,\mu$m. These two terms ($\sigma_{\rm sys,sub}$ and $\sigma_{\rm sys,main}$) should be summed up (rather than taking the root sum square), and thus the total systematic error in the antenna structure is $\sigma_{\rm sys,ant} = -124\,\mu$m, which represents the worst case at an EL of 15°. Note that for a higher EL angle, the systematic error could be reduced because the gravitational deformation would be less significant. For instance, at an EL larger than 45°, the systematic error is estimated to be $\sim 90\,\mu$m, or smaller.

In addition to the systematic error that occurs in the antenna structure, the errors in the noise source positions also cause a systematic error through a calculation error of the bias term, $l_{\rm bias}$. Assuming a position error of ~ 1 mm, the bias term error is estimated to be $38\,\mu$m for each noise source. Since the position errors are totally uncorrelated among the four noise sources, the systematic error introduced by the bias term error is $\sigma_{\rm sys,bias} = 19\,\mu$m ($= 38\,\mu{\rm m}/\sqrt{N_{\rm NS}}$) when the mean path difference of the four noise sources is considered.

A remaining factor that we must consider is the effect of the pointing error. Under the existence of a pointing offset, there should be an additional phase offset caused by a beam offset. According to a model calculation, this phase shift is $\sigma_{\rm sys,pnt} \sim 20\,\mu$m for a $20''$ pointing offset for the Q band (note that the typical dual-beam offset angle is $\sim 7''$–$15''$, and thus this also corresponds to the worst case). For the K band, in which the beam size is larger 2 times than that of the Q band, the offset is at the level of $\sim 10\,\mu$m. To obtain a final value of the systematic error, we take an rss (root sum square) of $\sigma_{\rm sys,ant}$, $\sigma_{\rm sys,bias}$, and $\sigma_{\rm sys,pnt}$ (the latter is not directly correlated with the gravitational deformation) to obtain $\sigma_{\rm sys} = (\sigma^2_{\rm sys,ant} + \sigma^2_{\rm sys,bias} + \sigma^2_{\rm sys,pnt})^{1/2} = 127\,\mu$m. This number is fairly close to our target accuracy of 0.1 mm and within an acceptable range of systematic errors. In fact, an order estimate of the astrometric error by $\sigma_{\rm sys}/B$, where $B = 2300$ km is the maximum baseline length of the VERA array, provides $\sigma_{\rm sys}/B \approx 11\,\mu$as.

If one takes into account both the statistical and systematic errors, the total error of the path-length calibration would be obtained as $\sigma_{\rm tot} = (\sigma^2_{\rm stat} + \sigma^2_{\rm sys})^{1/2} = 145\,\mu$m. However, any statistical errors can be significantly reduced by increasing the number of measurements. For instance, in practical radio observations, the four noise sources are powered on and off in turn every ~ 30 s, and thus the dual-beam path difference is determined every 2 min by taking an average of the four noise sources. Therefore, for a full 8 hr track observation, one should obtain more than 200 measurements of the mean path length, which would significantly reduce the effect of $\sigma_{\rm stat}$.

Another possible source of error is thermal expansion of the antenna structure. For instance, at the Mizusawa station where the seasonal temperature variation is the largest among the VERA stations, the difference of the highest and the lowest temperatures through the year is ~ 40°C. Using the expansion coefficient of steel 1.2×10^{-5}, such seasonal variations in temperature would cause a shift of the noise source positions by $1.2 \times 10^{-5}/^{\circ}{\rm C} \times 40^{\circ}{\rm C} \times 2.2\,{\rm m} \approx 1.1$ mm, where 2.2 m is the radius of the feedome base. Such a position shift could cause a change of the bias term by $\sim 42\,\mu$m in the worst case. However, we note that the effect of the thermal expansion of the feedome base is common to the four noise sources (i.e., basically the position shift occurs along the radial direction from the antenna axis with a similar amount of displacement). Hence, due to the symmetric location of the noise sources, the errors of the bias term should mostly cancel out (e.g., in table 1, the bias terms for each noise source have an FR angle offset of 90°), and thus only higher-order terms should remain as long as the mean of the four noise sources is taken.

In summary, the error in VERA's dual-beam delay calibration is likely to be dominated by the systematic error described above, which is $\sigma_{\rm sys} = 127\,\mu$m. The effect of the calibration error on VERA's astrometry is discussed later.

7. 10 m–20 m Experiment

In order to provide an ultimate confirmation of the validity of the horn-on-dish method, we conducted an experimental test of calibrations using an antenna pair at the Mizusawa station. At Mizusawa, a 10 m radio telescope, which is mainly used for geodetic observations, is located next to the VERA 20 m antenna, with a separation of ~ 30 m (see figure 8). By comparing fringe phases of a celestial object correlated between the 10 m antenna and the two beams of the 20 m (based on fast switching of VERA's dual-beams), one can measure the dual-beam delay difference between beams A and B of VERA 20 m, and then it can be directly compared with the dual-beam delay difference measured with the noise sources. An experiment was made on 2005 April 15, by observing the Orion KL H_2O maser at 22 GHz. We observed the source with both the 10 m and 20 m antennas at the same time for ~ 1 hr from 06:12 UT, and the correlation between the two telescopes was maintained to obtain fringe phases of the Orion KL H_2O maser. The typical source elevation angle was ~ 45°. The sky frequency was 22.227 GHz, and at each antenna the outputs of the two 16-MHz baseband channels were recorded onto magnetic tapes with the VSOP terminal, and correlated with the Mitaka FX correlator. For the VERA 20 m, beam A and beam B data were recorded onto the two channels, and for the 10 m, the same data were copied to the two channels, so that the correlations between VERA 20 m's beams A/B and 10 m were taken at one time with the Mitaka FX correlator.

During all of the experiments, VERA's dual-beam receivers were set to a $2.^{\circ}0$ separation ($\phi = 1.^{\circ}0$), and the 20 m antenna was rapidly switched every 30 s (i.e., a 60 s switching cycle) so that the Orion KL H_2O masers were observed with both beams A and B with a time difference of only 30 s (see figure 8 for a schematic view of the experimental setup). The switching was done by nodding the VERA 20 m telescope by rapidly driving the azimuth and elevation axes. Note that when the Orion KL H_2O maser was observed with beam A of the VERA 20 m telescope, beam B was directed toward the blank sky (and beam A toward the blank sky when observing the Orion KL H_2O maser with beam B). Since the pair separation angle of the dual-beam was 2°, the gravitational deformation change caused by the variation of the elevation angle (less than 2°) due to switching was negligible. To see the dependence of the calibration error on the field rotation angle, θ, during the

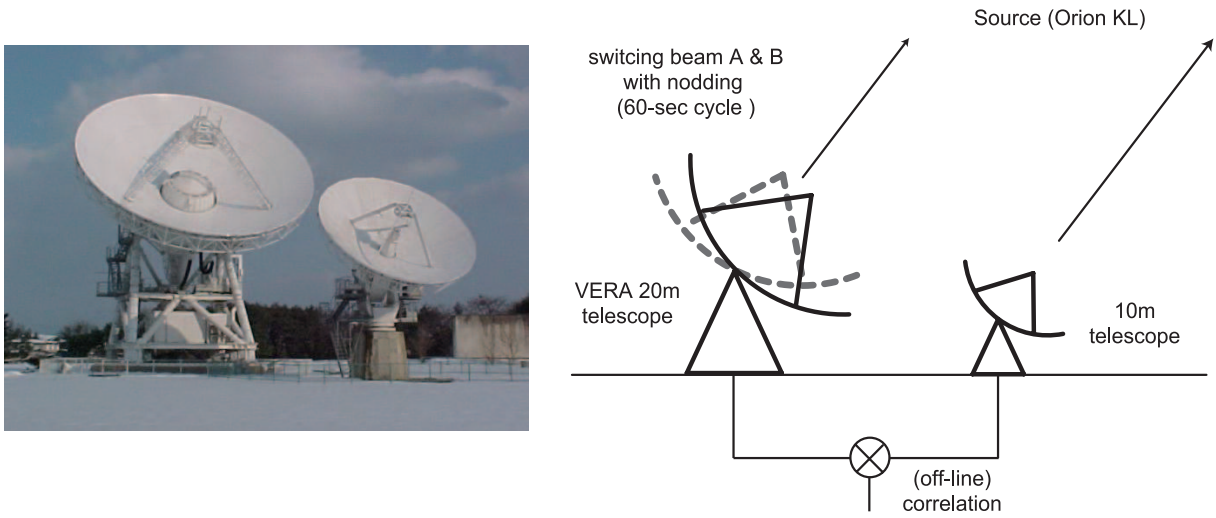

Fig. 8. Left: A picture of Mizusawa 10 m telescope and VERA 20 m telescope. Right: A schematic view of the 10 m–20 m experiment. Both the 10 m and 20 m telescopes observed the common source (Orion KL H_2O maser). During the observations, the VERA 20 m telescope was nodding so that the source is observed with beams A and B in turn with 60 s cycle.

observations we varied θ from 180° to −180° with every 45°, and at each θ data were taken for 3 switching cycles (3 min).

The direct observable quantity of Orion KL is the fringe phase between the 10 m and 20 m antennas' A beams ($\phi_{20\mathrm{A}-10}|_{\mathrm{obj}}$), and also that between their B beams ($\phi_{20\mathrm{B}-10}|_{\mathrm{obj}}$). In order to avoid any contamination of data that were taken during the antenna slew time, we used data for 16 s in the middle of 30 s half cycle to obtain $\phi_{20\mathrm{A}-10}|_{\mathrm{obj}}$ and $\phi_{20\mathrm{B}-10}|_{\mathrm{obj}}$. Since the H_2O maser source is very strong, the S/N ratio is typically ∼200 or larger, and thus is sufficiently high for calibration accuracy check at the level of 0.1 mm. Since the position error of the Orion KL H_2O maser (∼10″) caused only a small phase drift at a fringe rate of 10^{-5} Hz for a 30 m baseline, its effect is negligible in 1 min switching. To obtain these two fringe phases ($\phi_{20\mathrm{A}-10}|_{\mathrm{obj}}$ and $\phi_{20\mathrm{B}-10}|_{\mathrm{obj}}$) at one correlator path, two baseband channels of VERA's 20 m antenna were used to record the receiver outputs of beams A and B, and for the 10 m antenna the same data were recorded in the two baseband channels with its analog backends. Note that the use of the 10 m antenna's analog backends introduced an instrumental phase difference between the two channels of the 10 m antenna's output, which is denoted as $\Delta\phi_{10\mathrm{BA}}$. This kind of phase difference between baseband channels always occurs in analog VLBI backends, and is often calibrated with "P-Cal comb-tone signals". To calibrate $\Delta\phi_{10\mathrm{BA}}$ in this experiment, the phase difference between the two channels was measured by reversing the two channels of the 10 m anntenna's analog backends several times at both the beginning and the end of the 10 m–20 m experiment.

Using the fringe phases of the Orion KL H_2O maser obtained in the above-mentioned experiment, the path difference between the dual beams was obtained by taking an average of 3-cycle measurements, namely

$$\phi_{20\mathrm{B}-20\mathrm{A}}|_{\mathrm{obj}} = < \phi_{20\mathrm{B}-10}|_{\mathrm{obj}} - \phi_{20\mathrm{A}-10}|_{\mathrm{obj}} - \Delta\phi_{10\mathrm{BA}} > . \quad (25)$$

Here, the brackets, <>, indicate an average over 3 switching cycles, and the third term, $\Delta\phi_{10\mathrm{BA}}$, corresponds to the instrumental phase difference between the two baseband channels of the 10 m antenna's analog backends. The quantity, $\phi_{20\mathrm{B}-20\mathrm{A}}|_{\mathrm{obj}}$, corresponds to the dual-beam delay difference for a celestial object pair, i.e., $l_{\mathrm{inst,obj}}$ in equation (8). This should be compared with the dual-beam delay difference measured with the noise sources, that is, $l_{\mathrm{inst,NS}}$ in equation (9), which in this section we note as $\phi_{20\mathrm{B}-20\mathrm{A}}|_{\mathrm{NS}}$, in contrast to $\phi_{20\mathrm{B}-20\mathrm{A}}|_{\mathrm{obj}}$. During the 10 m–20 m experiment, the calibration noises were also injected into the dual-beam receivers of the VERA 20 m antenna, and $\phi_{20\mathrm{B}-20\mathrm{A}}|_{\mathrm{NS}}$ was monitored on real time. The difference $\phi_{20\mathrm{B}-20\mathrm{A}}|_{\mathrm{NS}}$ was evaluated for each noise source by subtracting the bias term, l_{bias}, which is known a priori.

Figure 9 shows the results of the 10 m–20 m experiment, presenting the dual-beam delay difference (described in phase rather than in length) for Orion KL ($\phi_{20\mathrm{B}-20\mathrm{A}}|_{\mathrm{obj}}$) and those for the noise sources ($\phi_{20\mathrm{B}-20\mathrm{A}}|_{\mathrm{NS}}$) against the FR angle θ. In figure 9, the dual-beam delay difference shows a sinusoidal variation with its peak at $\theta = 0°$, being consistent with those expected from the gravitational deformation. The amplitude of the dual-beam delay difference is ∼15°, corresponding to 560 μm. Therefore, the results given here confirm that the systematic error would easily exceed our target calibration accuracy of 0.1 mm if there were no calibration system using the horn-on-dish noise sources. However, as can be seen in the top panel of figure 9, basically the phases obtained by the noise sources (shown with symbols) are in agreement with those of Orion KL (dashed line with filled circles). In the bottom panel of figure 9, the phase differences between the celestial object and the noise sources ($\phi_{20\mathrm{B}-20\mathrm{A}}|_{\mathrm{obj}} - \phi_{20\mathrm{B}-20\mathrm{A}}|_{\mathrm{NS}}$) are plotted. For nine independent measurements of θ (for $\theta = -180°, -135°, ..., 180°$), the rms phase difference of each noise source ranges from 3.°5 to 5.°1, corresponding to 130 μm to 192 μm. Also, the average of the four noise sources is shown (dotted curve), which has an rms of 3.°1 in phase or 118 μm in path length. Therefore, this experiment confirms that the

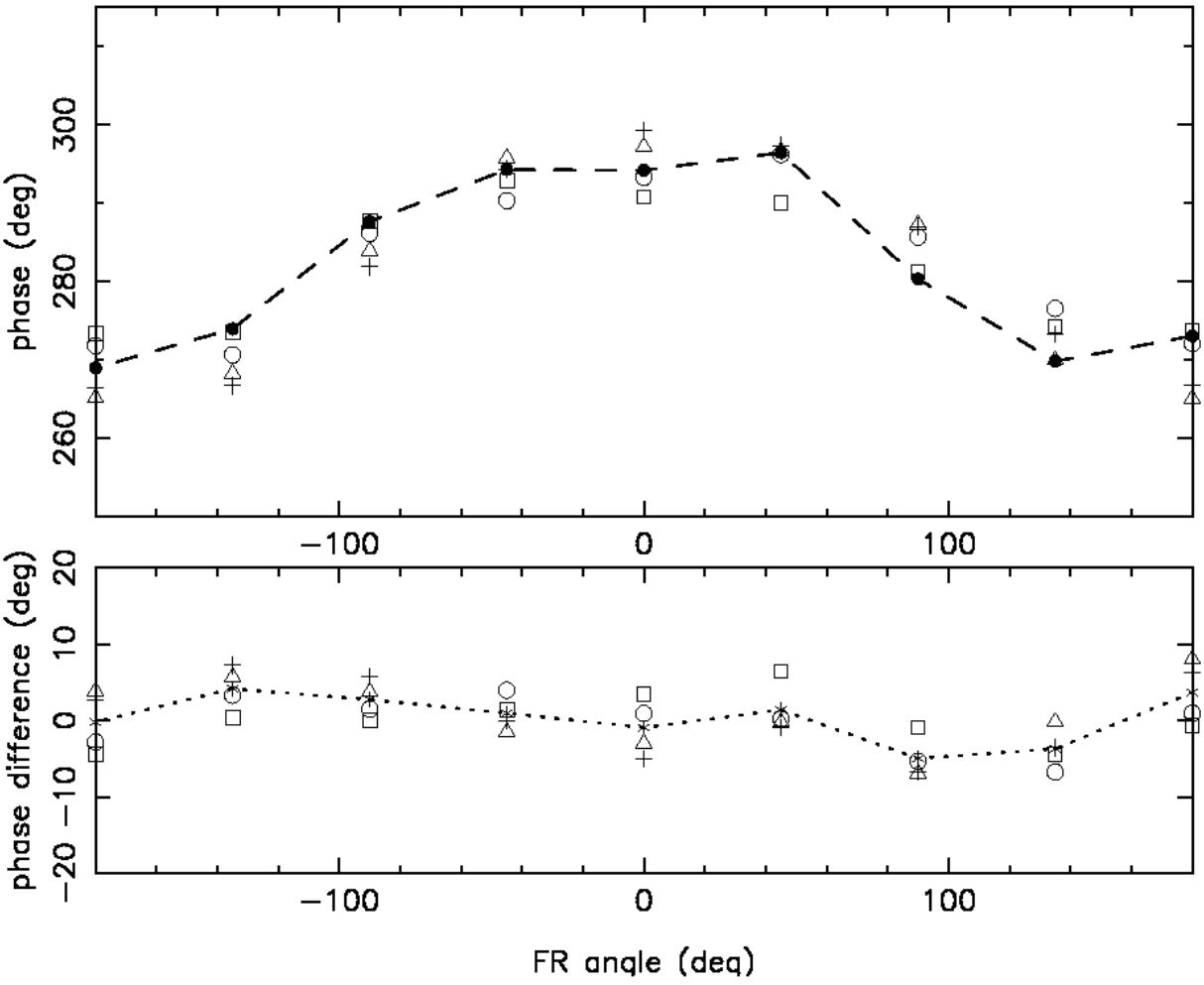

Fig. 9. Instrumental delay differences of the dual-beam measured with the noise sources and Orion KL in the 10 m–20 m experiment. Note that the measured phase data are shown in units of degree, In top panel, measured phases are plotted against the field rotation angle θ. For the noise source phases ($\phi_{\rm 20B-20A|NS}$), open circles are for NS1, squares for NS2, triangles for NS3, and crosses for NS4. Dashed line with filled circles shows the phases for Orion KL ($\phi_{\rm 20B-20A|obj}$). Bottom panel shows the difference in phase between the noise sources and Orion KL. Dotted curve corresponds to the mean of the four noise sources.

horn-on-dish method can indeed calibrate the dual-beam delay difference at a level requisite for the VERA projects.

Note that in the above experiment, the systematic errors discussed in the previous section (such as a dual-beam delay difference caused by the main reflector and the path difference between the noise sources and the celestial object) are also included in the phase of Orion KL, $\phi_{\rm 20B-20A|obj}$. As discussed in section 6, these terms could cause a systematic calibration error of $\sim 127\,\mu$m at the most, being consistent with the results of the 10 m–20 m experiment presented above (an rms of $118\,\mu$m using the mean of the four noise sources). In the bottom panel of figure 9, the phase difference ($\phi_{\rm 20B-20A|obj} - \phi_{\rm 20B-20A|NS}$) shows a rather sinusoidal systematic variation with respect to θ, which implies that the displacements of subreflector/main-reflector or receiver feed-horns are likely to be sources of the residuals seen here (rather than random noises). Note that the residual peak does not necessarily coincide with $\theta = 0^\circ$ or 180°, which may indicate that there could also be a small, but unknown, displacement of the main reflector, subreflector, or receiver feed-horns other than in the direction of gravity.

In these measurements, we note that the residual of the tropospheric fluctuations is also included in the results shown in figure 9. This residual originates from the fact that the two antennas are geometrically separated by ~ 30 m. We note that this residual is close to that expected for normal astrometric observations with VERA's dual beam. In fact, if one assumes a typical effective height of tropospheric water vapor of 1 km (e.g., Thompson et al. 2001), the pair separation angle of 2° corresponds to a spatial scale of 35 m at a height of 1 km. In contrast, in the 10 m–20 m experiment, the beams of the two antennas were parallel to each other (i.e., the two antennas are observing the same source Orion KL), and thus the tropospheric fluctuation difference on an ~ 30 m scale remained in the observed phase in Orion KL. Since these spatial scales are similar to each other, the residuals of tropospheric fluctuations for the 10 m–20 m experiment and normal astrometric observations with VERA's dual-beam should be similar. Therefore, the results presented in figure 9 ensure that the VERA system can calibrate the dual-beam instrumental

delay and phase errors caused by tropospheric fluctuations sufficiently for the accurate astrometry at the level of 10 μas.

8. Implication for Astrometry with VERA

8.1. Expected Astrometric Accuracy

As discussed in the previous sections, the expected systematic error in the calibration, $\sigma_{\rm sys}$, does not exceed 0.127 mm. When combined with the maximum baseline length of the VERA array, this corresponds to an astrometric error of 11 μas. We note that the systematic error, $\sigma_{\rm sys}$, is likely to be further reduced in multiepoch astrometry, since it is dominated by a gravitational deformation of the antenna structure, as described in section 6. For instance, in practical radio observations, multiepoch observations of a pair source are conducted with the same schedule (i.e., the same local sidereal time range), and thus the gravitational deformation effect is basically common to all epochs. Thus, the systematic effect is likely to cancel out in multiepoch astrometric measurements of parallax and proper motion. The only effect is that the systematic error of $\sigma_{\rm sys} = 127\,\mu$m could cause an offset on the order of $\sim 11\,\mu$as in the absolute position of the source, but measuring the absolute position with such a high accuracy is beyond the scope of our main purpose of VERA. With these facts and the maximum error given above ($\sigma_{\rm sys} = 127\,\mu$m, corresponding to an astrometric error of 11 μas), we conclude that the horn-on-dish method can calibrate the delay difference in the dual-beam system at a sufficient level for VERA's high-precision astrometry, and thus Galaxy-scale astrometry can be readily done with VERA as far as the calibration of the dual-beam delay difference is concerned.

We note that when discussing the astrometric accuracy with VERA, in addition to instrumental delay calibration, one should also consider the residual of the tropospheric delay between a pair of sources. According to dual-beam experiments by Honma et al. (2003), after phase-referencing, the residuals of the tropospheric fluctuation show a behavior like a white phase noise for an arbitrary period, and thus can be reduced statistically by integration for longer time. In fact, Honma et al. (2003) showed that the residual of the tropospheric fluctuation for a pair of sources with $\sim 0.^\circ 6$ separation (or $\phi \sim 0.^\circ 3$) can be reduced below the level of 0.1 mm within 1 min integration. This result is consistent with the success of the 10 m–20 m experiment presented in the previous section, in which the tropospheric delay effect is also included. We note that currently the limiting factor of VERA's astrometric accuracy is the error in the tropospheric zenith delay (which is rather constant or slowly varying), which is caused by an air mass difference between the source pair. For low-elevation sources, this effect is serious, and its error is much larger than the calibration error of the dual-beam delay difference. For calibrating the tropospheric zenith delay, see Honma et al. (2008) for details.

8.2. Practical Way of Calibration

Here, we summarize a practical way of a dual-beam delay calibration in VERA to provide a clear view of the calibration process to (future) users of VERA. In dual-beam observations, usually the four noise sources are powered on and off in turn every ~ 30 s during observations of a celestial object pair. Thus, every 2 min one can obtain the mean of the dual-beam delay difference from the four noise sources. This cycle period is controlled by the observation schedule, and can thus be modified (though on/off every 30 s is optimum). When the correlation process was finished, VERA observers will receive the correlated visibilities of the celestial object pair as well as the calibration tables, which are the dual-beam delay difference measured with the noise sources. The dual-beam delay differences in the tables are corrected for the bias term, i.e., obtained as

$$l_{\rm inst,NS} \equiv l_{\rm ant,NS} + l_{\rm RX} = l_{\rm obs,NS} - l_{\rm bias}. \quad (26)$$

The tables contain lists of $l_{\rm inst,NS}$ for each noise source and for the mean of the four noise sources. The best is, of course, to use the mean of the four noise sources, but tables for each noise source are also attached for some special cases, for instance, a trouble with one of the noise sources, etc. The tables are presented in a text format, and are also readable with AIPS. When applying the fringe solutions of the reference source to the target one, the calibration tables should also be applied to correct for the dual-beam delay difference, and then a phase-referenced map can be obtained from the phase-referenced visibilities. Note that while the $l_{\rm ant,NS}$ term is on the order of ~ 0.5 mm as a typical case (e.g., the amplitude of sinusoidal curve in figure 9), $l_{\rm inst,NS}$ is totally unpredictable, because it includes a transmission cable length and a local oscillator phase ($l_{\rm RX}$), and thus implementation of the horn-on-dish calibration is always necessary, regardless of the target accuracy of astrometry.

The authors would like to thank the referee, Dr. Leonid Petrov, for careful reading and constructive suggestions, which improved this paper. We are also grateful to the members of Communication Systems Center of Mitsubishi Electric Corporation for the antenna design and their supports in studying the calibration technique, particularly in the early stage of research and development.

References

Honma, M., et al. 2003, PASJ, 55, L57
Honma, M., Kawaguchi, N., & Sasao, T. 2000, Proc. SPIE, 4015, 624
Honma, M., Tamura, Y., & Reid, M. J. 2008, PASJ, 60, 951
Kawaguchi, N., Sasao, T., & Manabe, S. 2000, Proc. SPIE, 4015, 544
Kobayashi, H., et al. 2008, in Proc. IAU Symp., vol. 248, ed. W. J. Jin, I. Palatis, & M. A. C. Perryman (Cambridge: Cambridge University Press), 148
Otoshi, T. Y. 1981, Telecommunications and Data Acquisition Progress Report (NASA/JPL), 42-66, 49[2]
Thompson, A. R., Moran, J. M., & Swenson, G. W., Jr. 2001, Interferometry and Synthesis in Radio Astronomy, 2nd ed. (New York: John Wiley & Sons), chap. 9

[2] ⟨http://ipnpr.jpl.nasa.gov/progress_report/42-66/66I.PDF⟩.